Biological and clinical significance of the AGE-RAGE axis in the aggressiveness and prognosis of prostate cancer

Recommended Citation

Biological and clinical significance of the AGE-RAGE axis in the aggressiveness and prognosis of prostate cancer

Shih-Hong Khoo [a,1], Pei-Ru Wu [b,c,1], Kun-Tu Yeh [c,d,e], Shih-Lan Hsu [f], Chi-Hao Wu [g,*]

[a] School of Nutrition and Health Sciences, College of Nutrition, Taipei Medical University, Taipei 110301, Taiwan
[b] Department of Pathology, Cheng-Ching General Hospital, Taichung 40764, Taiwan
[c] Department of Surgical Pathology, Changhua Christian Hospital, Changhua 50006, Taiwan
[d] School of Medicine, Chung Shan Medical University, Taichung 40201, Taiwan
[e] Department of Post-Baccalaureate Medicine, College of Medicine, National Chung Hsing University, Taichung 40227, Taiwan
[f] Department of Medical Research, Taichung Veterans General Hospital, Taichung 40705, Taiwan
[g] Graduate Program of Nutrition Science, School of Life Science, National Taiwan Normal University, Taipei 11677, Taiwan

Abstract

Dietary factors and chronic hyperglycemia are linked to the formation of advanced glycation end products (AGEs) and prostate cancer (PCa) risk. The activation of the receptor for AGEs (RAGE) acts as a bridge between various RAGE ligands and certain malignancies. This study showed that the interaction of AGEs and RAGE promoted PCa cell proliferation, invasion, and autophagy-mediated survival in response to chemotherapeutic agents. RAGE-overexpressed PCa cells underwent epithelial−mesenchymal transition and showed increased cancer stem cell-like properties. In mouse xenograft models, RAGE-overexpressed cells showed more substantial tumorigenic capacity than parental cells, whereas RAGE knockdown decreased tumorigenicity. The clinical data validated a positive correlation between high AGE and RAGE expressions with poor clinical outcomes. Our findings suggest that the AGE-RAGE axis facilitates PCa progression and aggressiveness. Prostatic AGEs and RAGE expression levels are associated with PCa prognosis. Adherence to a reduced-AGE diet and targeting RAGE are potential approaches to complement and synergize with the current PCa therapies.

Keywords: Advanced glycation end products, Aggressiveness, Glycative stress, Prostate cancer, RAGE

1. Introduction

Advanced glycation endproducts (AGEs) are nonenzymatic browning products derived from the glycation of carbonyl groups on reducing sugars and amino groups on proteins [1]. Cooking foods at high temperatures or processing them extensively can accelerate the formation of AGEs. Research studies have shown a positive correlation between the levels of circulating AGEs and the amount of AGEs present in the foods consumed. Approximately 10% of dietary AGEs are absorbed by the small intestine and enter the bloodstream, of which about one-third are excreted through urine within 72 h, and the rest remain in the body [2]. These exogenous AGEs have been associated with the induction of oxidative stress and inflammation, heightening the risk of developing cancer [3].

Biological sugars and sugar metabolites, such as glucose (GLU), fructose, glyceraldehyde (GA), glycolaldehyde (GOA), glyoxal (GO), and methylglyoxal (MG), play a role in glycation reactions and impact the types of AGEs formed [4]. Patients with diabetes have significantly higher AGE levels due to their persistent hyperglycemia conditions [5]. Currently, up to 40 AGEs have been characterized in the body, including argpyrimidine, Nε-(carboxyethyl)-lysine, Nε-(carboxymethyl)-lysine (CML), (S)-2-amino-5-(5-methyl-

4-oxo-4,5-dihydro-^{1}H-imidazole-2-ylamino) pentanoic acid, pentosidine, and pyrraline [2]. Notably, the glycation process can form reactive carbonyl species (RCS), such as GO and MG [6]. RCS are toxic to cells with high glycation reactivity, which causes carbonyl stress and low-grade inflammation [7].

The binding of AGEs to the receptor for AGE (RAGE) triggers the NF-κB signaling cascade, leading to oxidative stress and initiating the secretion of IL-1β, IL-6, TNF-α, and HMGB1, fueling inflammation in the tumor microenvironment. These positive feedback loops may continuously stimulate tumor proliferation and progression [8]. Adherence to unhealthy dietary patterns, such as high-sugar, high-fat, and ultra-processed foods, is associated with increased AGE exposure [9]. Consuming deep-fried foods more than once a week increases the risk of PCa by 37% [10]. A recent meta-analysis of 25 prospective studies showed that consumption of a large amount of processed meat increases the risk of developing PCa [11]. High sugar-sweetened beverages may increase the risk of PCa- and obesity-related cancers [12]. Certain foods containing refined sugars, fats, and processed meat have been classified as foods with a high dietary inflammatory index. They are considered the risk factors for PCa among Italians [13]. Asians living in Asia have a much lower PCa incidence than those living in North America, showing that PCa may be associated with dietary patterns [14].

This study conducted the *in vitro* and *in vivo* experiments to evaluate the biological impacts of the AGE-RAGE axis in PCa hallmarks. Given that dietary pattern is a modifiable risk factor of PCa, choosing a low-AGE diet and targeting RAGE in the clinical setting could be potential therapeutic options for advanced PCa.

2. Materials and methods

2.1. Materials

The chemicals, recombinant proteins, and antibodies used for Western blot, co-immunoprecipitation, and immunofluorescence are listed in Supplementary Table 1 and Table 2. All chemicals and solvents used were of analytical grade.

2.2. Preparation and characterization of AGEs-BSA

Preparation of GLU-, GA-, GO-, GO, and MG-derived AGE was based on the work of Takeuchi et al. [15] as described in the Supporting Information and Supplementary Fig. S1.

2.3. Cell lines, cell culture, and cell viability

The human PCa cell lines 22rv1 and LNCaP (androgen-dependent), DU145 and PC3 (androgen-independent), CA-HPV-10 (prostatic adenocarcinoma of Gleason grade 4/4), and PZ-HPV-7 (epithelial cells from the peripheral zone of the normal prostate) were obtained from the Bioresource Collection and Research Center (Food Industry Research and Development Institute, Taiwan). Human primary prostate epithelial (HuPPE) cells were purchased from ABM (T4078, BC, Canada). All cells were cultured in RPMI 1640 medium supplemented with 1% L-glutamine and 10% fetal bovine serum (FBS, Gibco Life Technologies, Grand Island, NY, USA) at 37 °C under an atmosphere of 5% CO_2. The detailed information for measuring cell viability was described in the Supporting Information.

2.4. Plasmids and stable transfections

Stable RAGE and HMGB1 overexpression and knockdown clones, as well as ATG5 and BECN1 knockdown clones from DU145 and PC3 cells were generated by transfecting the indicated plasmids as described in the Supporting Information. Total protein lysates (20 μg) from antibiotic-selecting cells were analyzed using Western blot or immunofluorescence for monitoring target protein expression. In this study, RAGE-transfected DU145 cells were classified as RAGE low-expressing (R^L) clones, medium-expressing (R^M) clones, and high-expressing (R^H) clones based on the RAGE expression level. DU145-R^H clones were subjected to RAGE shRNA plasmid transfection to generate shR^H subclones for subsequent experiments (Supplementary Fig. S2).

2.5. Immunofluorescence staining

A total of 2×10^4 cells were cultured in a μ-Slide 8 Well chamber (ibidi, Germany) and then fixed with 4% formaldehyde at 24 °C for 15 min. After that, 0.1% Triton X-100 was added, and the cells were incubated at 24 °C for 15 min. The slides were immersed in PBS containing 5% BSA at RT for 1 h of blocking and probed with an anti-RAGE antibody (1:200) overnight at 4 °C. DAPI staining solution was used for labeling nuclear DNA, and a confocal microscope (Leica Microsystems, Wetzlar, Germany) was used to analyze the fluorescent images of cells.

2.6. Immunoblotting and co-immunoprecipitation (co-IP)

Western blot and co-IP were performed as previously reported [16] as described in the Supporting

Information. Protein expression was measured densitometrically compared to the loading control reference band using a Fusion Solo System (Vilber Lourmat, Germany) and ImageJ software.

2.7. Detection of acidic vesicular organelles (AVOs) and GFP-LC3 puncta

Acridine orange dye (A3568, ThermoFisher Scientific) was used to evaluate the formation of AVOs in the PCa cells. Briefly, 3×10^4 cells cultured in a μ-Slide 4 Well chamber (ibidi) were treated with DTX for 16 h, stained with acridine orange (1 μg/mL), and covered in a complete medium containing 10% FBS. The formation of AVOs in cells was detected using the EVOS FL Auto Imaging System (Thermo Fisher Scientific). For the detection of GFP-LC3 puncta, PCa cells were transfected with pSELECT-GFP-LC3 plasmids (#10K02-MM, InvivoGen) to stably express the GFP-LC3 fusion gene and maintained under Zeocin (ant-zn-05, InvivoGen) selection in RPMI-1640 with 10% FBS at 37 °C in 5% CO_2. DU145 clones with different expression levels of RAGE were treated with DTX for 16 h. GFP-LC3 puncta was imaged using a confocal microscope (Leica Microsystems).

2.8. Measurement of HMGB1 release

HMBG1 release in culture media was measured by an HMGB1 ELISA Kit (326078738, Shino-Test Corporation, Kanagawa, Japan) following the manufacturer's instructions. The detection range of the HMGB1 was 1−80 ng/mL.

2.9. Transmission electron microscope (TEM)

A total of 3×10^4 DU145 cells were cultured in a 4-well chamber slide (ThermoFisher Scientific). After overnight adhesion, the culture medium was changed, DTX (10 nM) was added, and the cells were incubated for 16 h. Cell samples were processed for fixing, dehydration, embedding, and sectioning at Taipei Medical University Core Facility. In addition, TEM (HT-7700, Hitachi, Japan) was used to detect autophagic structures.

2.10. Matrigel invasion transwell assays

Nunc Cell Culture Inserts in Carrier Plate Systems (141006, ThermoFisher Scientific) were used for cell invasion assays as previously reported [17]. A 0.2% crystal violet stain solution was used to stain the cells. The invaded crystal violet-stained cells were counted using the EVOS FL Auto Imaging System (ThermoFisher Scientific).

2.11. Side-population (SP) and ALDEFLUOR assays

For the SP assay [18], parental, R^H, and shR^H DU145 cells were divided into three groups at a density of 1×10^6 cells. The first and second groups were treated with the ATP-binding cassette transporter inhibitors reserpine and verapamil for 30 min at 37 °C, respectively. All groups were cultured in a complete medium and labeled with Hoechst 33342 (5 μg/mL) at 37 °C for 90 min. Subsequently, the cells were pelleted via centrifugation at 4 °C and resuspended in cold PBS to avoid dye degradation. Cells were labeled with 2 μg/mL PI before flow cytometry analysis to discriminate between live and dead cells. The SP and non-SP cells were analyzed and sorted using a FACSCanto II (BD Biosciences, Mountain View, CA, USA) with excitation at 355 nm and emission at 450 and 675 nm. SP cells were detected as distinct Hoechst 33342^- within PI^- cells. Aldehyde dehydrogenase (ALDH) activity was measured using the ALDEFLUOR kit (StemCell Technologies, Durham, NC, USA) according to the manufacturer's instructions. Aliquots of $ALDH^+$ and $ALDH^-$ cells were evaluated using a FACSCanto II flow cytometer (BD Biosciences). The cell concentration of 1×10^5 cells/mL in assay buffer was subjected to the ALDEFLUOR assay and 10,000 cells were recorded. Diethylaminobenzaldehyde (DEAB, 7.5 μM), a pan-inhibitor of ALDH, was used as a control for background fluorescence.

2.12. Animals

Three-to four-week-old male NOD/SCID (n = 15) and nude (n = 15) weighing 20−25 g were purchased from BioLASCO Taiwan Co., Ltd. Mice were maintained in the following specific pathogen-free standard housing conditions: temperature-controlled room (22 ± 2 °C), 50 ± 10% humidity, and a 12 h−12 h light−dark cycle (0600−1800) with food and water *ad libitum*). All animal experiments were conducted following the Guide for the Care and Use of Laboratory Animals (National Academy of Sciences, Taiwan) and approved by the Institutional Animal Care and Use Committee of Taipei Medical University (No. LAC-101-0236).

2.13. Xenograft murine models

Stably expressed firefly luciferase was generated by transfecting DU145 cells with pGL4.51[luc2/

CMV/Neo] vectors (E1320, Promega). Xenograft experiments were performed with 5-week-old NOD/SCID mice. The animals were randomized into three groups: the first group was injected with DU145 parental cells (P), the second group with the R^H clone, and the third group with the shR^H subclone. Each group consisted of five animals. PCa cells (1×10^6) were diluted into 100 μL of PBS and Matrigel (BD Biosciences) mixture and subcutaneously injected into the flank of each mouse. Tumor growth was monitored weekly with the IVIS Lumina XRMS In Vivo Imaging System (PerkinElmer, Waltham, MA, USA) for 4 weeks. To evaluate the tumor-initiating capacity of SP cells, the SP and non-SP cells from the DU145-R^H clone were sorted by the FACS AriaIII flow cytometer (BD Biosciences) and resuspended at 1×10^4 cells with Matrigel (BD Biosciences). The cell-Matrigel mixture was subcutaneously injected into the flanks of nude mice under anesthesia and monitored weekly for up to 10 weeks. During the experiment, no mice were euthanized, as none experienced a >20% decrease in body weight.

2.14. Patients with PCa and clinical tissues

Seventy-two PCa tissue samples were obtained from the Changhua Christian Hospital tissue banks in Taiwan to evaluate the association of CML and RAGE expression levels with clinical/pathological factors and survival. The demographic characteristics and medical information were obtained from their medical records. The tumors were graded and classified according to the guidelines outlined by the American Joint Committee on Cancer (AJCC), 7th edition [19]. All research protocols were approved by the Institutional Review Board (IRB) of Changhua Christian Hospital (IRB No. 140101, date of approval: March 5, 2014), the informed consent committee on human subjects, and the biospecimen unitization committee. This retrospective study was conducted according to the Declaration of Helsinki and HIPPA-approved protocols based on the highest ethical standards and the IRB.

2.15. Immunohistochemistry (IHC) staining and analysis

The HE and IHC staining of human PCa tissues were described in the Supporting Information. The IHC staining sections were scored using a semi-quantitative scoring system by two independent histopathologists (Dr. Pei-Ru Wu and Dr. Kun-Tu Yeh) in a double-blind setup. The CML and RAGE expressions were divided into low- and high-expression groups based on scores of 0−1 and 2−3, respectively. No cytoplasmic staining was scored as 0, mild cytoplasmic staining was scored as 1, moderate cytoplasmic staining was scored as 2, and strong cytoplasmic staining was scored as 3.

2.16. Statistical analysis

Data are presented as the means ± SD from three independent experiments. Statistical analyses were performed by one-way analysis of variance (one-way ANOVA) followed by Tukey's post hoc test for multiple comparisons using Prism 9 (GraphPad Software, Inc., San Diego, CA). A Student's t-test was used for two-group comparisons, with the level of statistical significance set at P < 0.05. Correlations among CML, RAGE, and clinicopathological parameters were calculated using Fisher's exact and chi-square tests. The Kaplan−Meier method with the log-rank test was performed to determine the overall survival (OS) curves and cumulative survival rate. These analyses were performed using SPSS software version 15.0 (SPSS Inc., Chicago, IL, USA).

3. Results

3.1. AGEs promote PCa cell proliferation and chemoresistance

This work prepared AGEs by incubating BSA with different glycated agents. The browning index, AGE-associated fluorescence, and SDS-PAGE were employed to estimate the degrees of glycation (Supplementary Fig. S1). Human androgen-dependent (22rv1 and LNCaP) and androgen-independent (DU145 and PC3) PCa cell lines were treated with AGEs (50−500 μg/mL) for 48 h. Among the five AGEs tested, GA- and GOA-derived AGEs promoted cell proliferation by 111−128% in androgen-dependent (Fig. 1A) and androgen-independent PCa cells (Fig. 1B). The treatment of anti-RAGE neutralizing antibodies (10 μg/mL) abrogated these proliferation-promoting effects (Fig. 1C). Under the chemotherapeutic drug DTX challenge, the treatment of GA- and GOA-derived AGEs (100 μg/mL) significantly increased the viability of LNCaP, DU145, and PC3 cells (Fig. 1D, P < 0.05). Among the five structurally identified AGE compounds, CEL and CML increased the resistance of PCa cells toward DTX (Fig. 1E). Preincubation of cells with 10 μg/mL sRAGE counteracted the CML-mediated chemoresistance in DU145 cells (Fig. 1F). These findings indicated that AGEs might promote PCa cell proliferation and enhance chemoresistance and
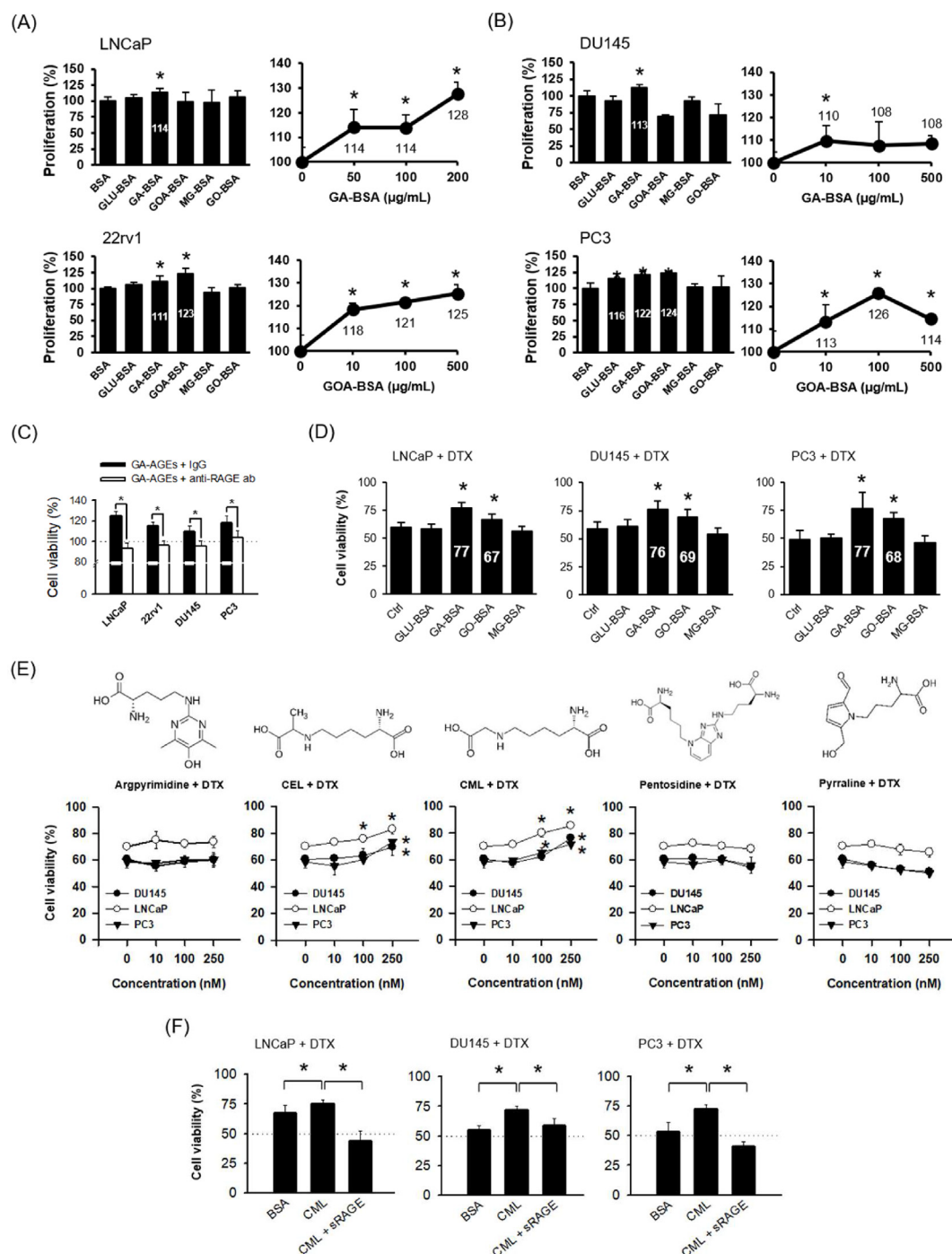
Fig. 1. *AGEs promote cell proliferation and decrease sensitivity to chemodrugs in PCa cells. (A) Androgen-dependent LNCaP and 22rv1, and (B) androgen-independent DU145 and PC3 cells were treated for 48 h with five types of AGEs-BSA (10–500 μg/mL) derived from different glycated agents. Cell viability was measured using the MTS assay and expressed as a relative percentage of the BSA control. GA-derived and GOA-derived AGEs increased PCa cell proliferation, whereas the other AGEs failed to enhance cell proliferation. (C) Treatment with anti-RAGE antibodies inhibited GA-derived AGEs-induced cell proliferation. PCa cells were co-treated with GA-derived AGE and anti-RAGE antibodies (10 μg/mL) for 48 h. Treatment of (D) AGEs-BSA (500 μg/mL) and (E) AGE compounds increased resistance to chemodrug toxicity in PCa cells. The cells were co-treated with AGEs and DTX (7.2 μM) for 24 h, and the cell viability was measured. GA-derived and GOA-derived AGEs, CEL, and CML increased PCa cell survival in response to the DTX challenge. (F) sRAGE counteracted CML-mediated chemoresistance and rendered PCa cells more sensitive to DTX toxicity. The cells were preincubated with sRAGE for 24 h, after which DTX was added and incubated for another 24 h. Data shown represents the means ± SD from three independent experiments with 6–8 replicates each. *P < 0.05 when compared with the BSA or vehicle control. DTX, docetaxel; anti-RAGE ab, anti-RAGE antibody; sRAGE, soluble RAGE.*

that the mechanism of action may involve the activation of RAGE.

3.2. RAGE confers chemoresistance in PCa cells

The levels of RAGE expression in normal human prostate cells and PCa cell lines were determined by Western blot. In Fig. 2A, androgen-independent DU145, and PC3 as well as prostatic adenocarcinoma CA-HPV10 cells had higher RAGE expression levels than those in androgen-dependent (22rv1 and LNCaP), HuPPE, and the normal prostate PZ-HPV7 cells. The data imply that PCa cells derived from aggressive castrate-resistant tumors exhibit high RAGE expression features. Following this, we generated stable RAGE overexpression and knockdown clones of PCa cells to investigate the function of RAGE on PCa hallmarks. The pUNO1-hager vector- and RAGE shRNA-transfected DU145 and PC3 cells were selected and characterized using western blotting. The empty pUNO1-mcs vector- and non-targeting control shRNA-transfected cells were served as the parental control (P). As shown in Supplementary Fig. S2, a total of 10 clones from DU145 were validated by Western blot, among which three clones with different RAGE expression levels were selected as high (R^H, clone 4), middle (R^M, clone 3), and low (R^L, clone 1) RAGE-expressing cells. For PC3, clone 3 was selected as having high RAGE expression (R^H) compared to the parental cells. The DU145- and PC3-R^H clones were further subjected to shRAGE transfection to generate shR^H subclones for subsequent investigations (Fig. 2B). Immunofluorescence staining showed that the expressions of RAGE appeared mostly at the cell boundaries and partially in the cytoplasm, indicating that RAGE is mainly expressed on the cell membrane (Fig. 2C).

The RAGE overexpression and knockdown clones were treated with chemodrugs for 24 h, and the cell viability was measured. The cell viability of DU145 (Fig. 2D) and PC3 (Fig. 2E) increased substantially with increasing RAGE expression. In contrast, RAGE knockdown rendered shR^H cells more sensitive to chemodrug toxicity. We also found that ERK phosphorylation and c-jun protein expression were increased in the RAGE-overexpressed clones (Supplementary Fig. S3). Pretreatment with RAGE (a mixture composed of anti-RAGE neutralizing antibodies and FPS-ZM1) or ERK (U0126, 10 μM) inhibitors sensitized DU145-R^H and PC3-R^H cells to the cytotoxic action (Fig. 2F). These findings suggest that overexpression of RAGE facilitates chemoresistance *in vitro* and that ERK could be a downstream signaling molecule coupled with RAGE.

3.3. RAGE-mediated chemoresistance relies on sustaining autophagy and limiting apoptosis

We further detected the expression of apoptosis and autophagy marker proteins to investigate the possible mechanism of RAGE-mediated chemoresistance under the DTX challenge. Fig. 3A showed that DTX induced caspase-3 and PARP cleavage in DU145 cells. In contrast, overexpression of RAGE inhibited the cleavage of these apoptotic proteins and promoted the conversion of LC3-I to LC3-II as well as p62 degradation for autophagy induction. The accumulation of GFP-LC3 punctate spots (Fig. 3B) and multiple acridine orange-stained regions (Fig. 3C) were observed in RAGE-overexpressed cells under DTX stress, indicating autophagy induction. As shown in Fig. 3D, TEM verified the ongoing autophagy at the ultrastructural level. There were fewer autophagic vacuoles in parental and R^L cells with or without DTX treatment. In R^H cells, autophagic vacuoles were more prevalent, and the bilayer degradative autophagic vacuoles (AVds) formed by the fusion of autophagic vacuoles and lysosomes were observed within the cytoplasm. Treatment with wortmannin, an autophagy inhibitor, sensitized the cytotoxic action of DTX in the parental and R^H clones of DU145 cells (Fig. 3E). Following this, we next generated stable BECN1, ATG5, and HMGB1 knockdown subclones from the R^H clone to validate the cytoprotective role of autophagy. Knockdown of BECN1 (Fig. 3F), ATG5 (Fig. 3G), and HMGB1 (Fig. 3H) enhanced the cytotoxic action of DTX on these cells. In summary, RAGE activation could trigger cytoprotective autophagy and evade apoptosis, while blockade of RAGE could increase susceptibility to chemotherapeutic agents.

3.4. RAGE triggers autophagy via inhibiting Akt/mTOR phosphorylation and facilitating BECN1—HMGB1 complex formation

To further understand the potential molecular mechanisms by which RAGE promotes autophagy, we analyzed Akt/mTOR signaling using western blotting. Fig. 4A showed that RAGE overexpressed R^H cells led to more significant inhibition of Akt and mTOR phosphorylation in response to DTX. The inhibition of phosphorylation was significantly abolished by RAGE knockdown (shR^H) ($P < 0.05$). The co-IP assay further proved that R^H cells promote the dissociation of Bcl-2 from BECN1 and facilitate BECN1-HMGB1 complex formation under DTX stress. Knockdown of RAGE (shR^H) sustained the BECN1-Bcl-2 complex and inhibited HMGB1 binding to BECN1 (Fig. 4B, upper panel). In
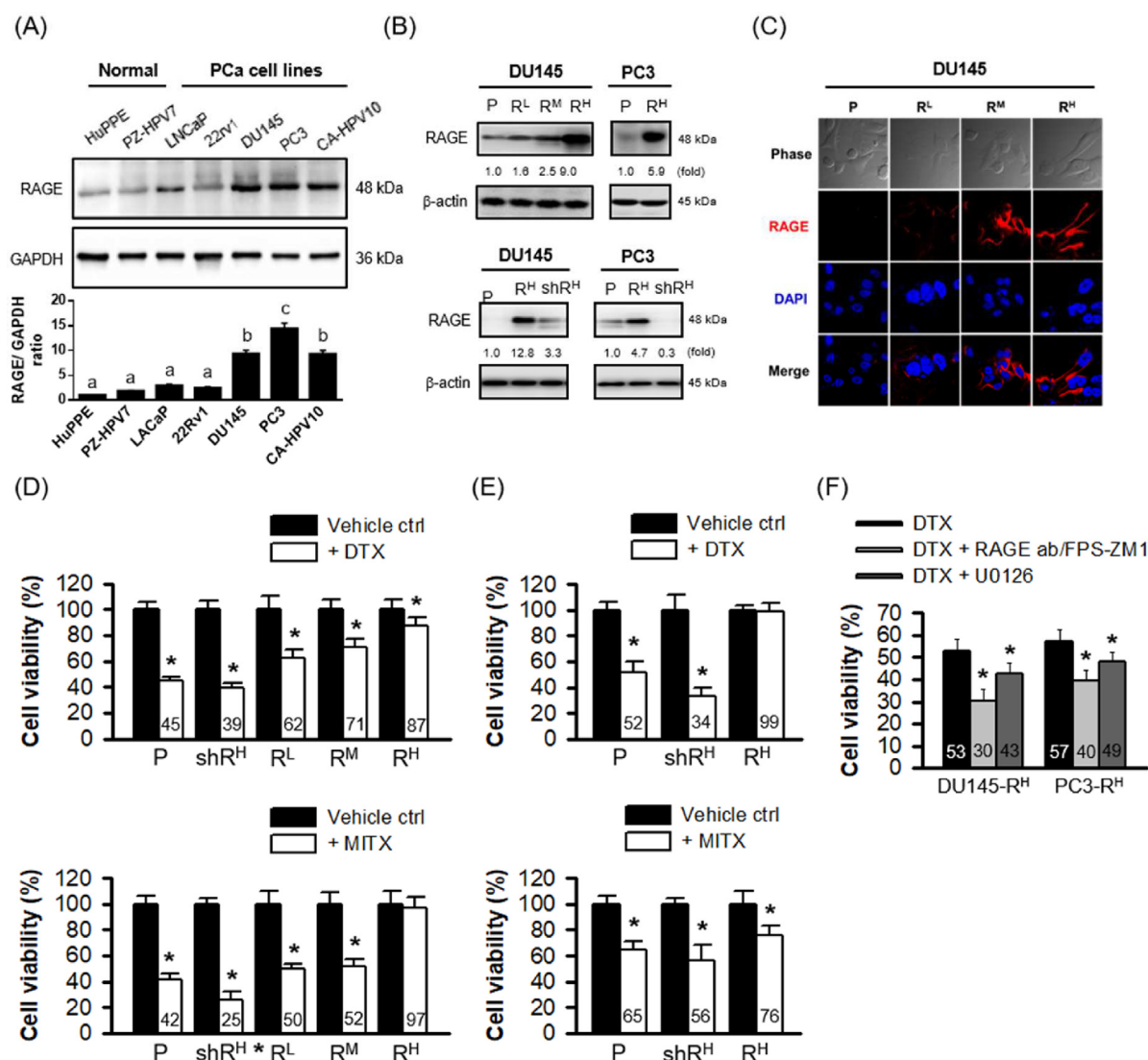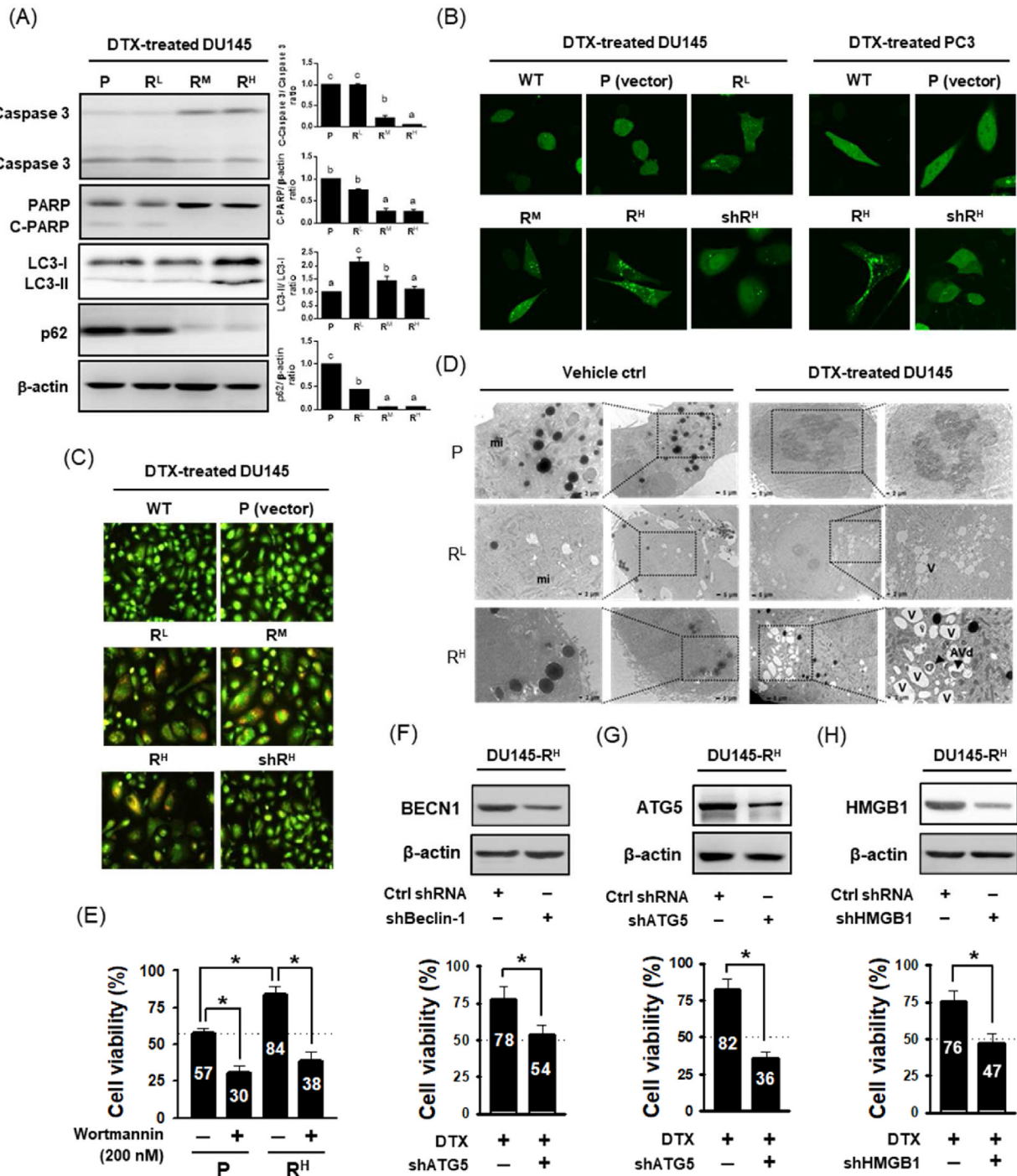
Fig. 2. RAGE overexpression enhances chemodrug resistance in PCa cells. (A) RAGE expression levels in normal and PCa cell lines were detected using western blotting. (B) Western blotting and (C) immunofluorescence staining were performed to validate the overexpression and knockdown of RAGE in the DU145 and PC3 cells, with β-actin used as the loading control. Stably RAGE-expressing DU145 cells were divided into low (R^L), middle (R^M), and high (R^H) clones based on the level of RAGE protein. R^H cells further subjected to shRAGE transfection were referred to as shR^H subclones. In PC3 cells, R^H and shR^H clones were also generated, as described above. An empty vector (pUNO1-mcs) and non-targeting control shRNA were used as the parental control (P). RAGE-overexpressed DU145 (D) and PC3 cells (E) showed increased resistance to chemodrug challenge. The cells were treated with DTX and MITX, respectively, for 24 h, and the cell viability was measured using the MTS assay. (F) Inhibition of RAGE or ERK sensitized RAGE-overexpressed cells to the DTX toxicity. The cells were pretreatment with RAGE (a mixture composed of anti-RAGE neutralizing antibody and FPS-ZM1) or ERK (U0126, 10 μM) inhibitors, and then treated with DTX for 24 h. Data shown represents he means ± SD from three independent experiments with 6−8 replicates each. *P < 0.05 when compared with the vehicle control. DTX, docetaxel; MITX, mitoxantrone.

addition, the expressions of autophagy-related proteins (LC3-II, Atg5−Atg12) were significantly upregulated in the RAGE-overexpressed cells, whereas Bcl-2 expression was significantly down-regulated (Fig. 4B, lower panel, P < 0.05).

To evaluate the potential of HMGB1 in the modulation of autophagy, we generated stable HMGB1 overexpression (HMGB1^H) and knockdown (shHMGB1) clones from DU145 cells. Interestingly, the HMGB1^H clone exhibited chemoresistance

properties towards DTX and MITX. In contrast, the HMGB1 blockade rendered the cells more susceptible to chemodrug toxicity (Fig. 4C and D). Treatment of DU145 cells with recombinant HMGB1 protein (10 ng/mL) was shown to rescue DTX- and MITX-induced cell death by 23% and 21%, respectively (Fig. 4E). Following this, the release of HMGB1 was measured in culture media using an ELISA assay kit. As shown in Fig. 4F, PCa cells were found to respond to DTX by releasing HMGB1. The

Fig. 3. RAGE triggers protective autophagy and limits apoptosis in response to the chemodrug stress. (A) Western blot analysis of autophagy- and apoptosis-related proteins in the RAGE-overexpressed clones of DU145 cells. The cells were treated with DTX (10 nM) for 24 h, and the cell lysates were analyzed with β-actin as a loading control. In DTX-treated cells, the number of GFP-LC3 puncta (B) and acridine orange-positive staining cells (C) were markedly increased in RAGE-overexpressed cells, whereas knockdown of RAGE (shR^H) counteracted these effects. The cells were treated with DTX (10 nM) for 24 h, followed by transfection with the GFP-LC3 vector for 4 h prior to imaging. GFP-LC3 puncta were detected using fluorescence microscopy. Acridine orange (1 μg/mL) was incubated with DTX-treated cells for 15 min. The formation of autolysosomal vesicles was detected using fluorescence microscopy. (D) Ultrastructural features of autophagic vacuoles (V) and degradative autophagic vacuoles (AVds) in DTX-treated PCa cells. The cells were treated with DTX (10 nM) for 16 h, followed by fixation and visualization using TEM. The accumulation of autophagic structures—V (early autophagy) and AVds (late autophagy) along with digested organelles was observed in the RAGE-overexpressed cells. (E) Pretreatment with the autophagy inhibitor Wortmannin (200 nM) and knockdown of (F) BECN1, (G) ATG5, and (H) HMGB1 augmented the DTX cytotoxicity in parental or RAGE-overexpressed cells. The cells were treated with DTX for 24 h, and cell viability was measured by an MTS assay. Data shown represents the means ± SD from three independent experiments. *P < 0.05 when compared with the vehicle control. AVds, degradative autophagic vacuoles; BECN1, Beclin 1; DTX, docetaxel; mi, mitochondria; TEM, transmission electron microscope.
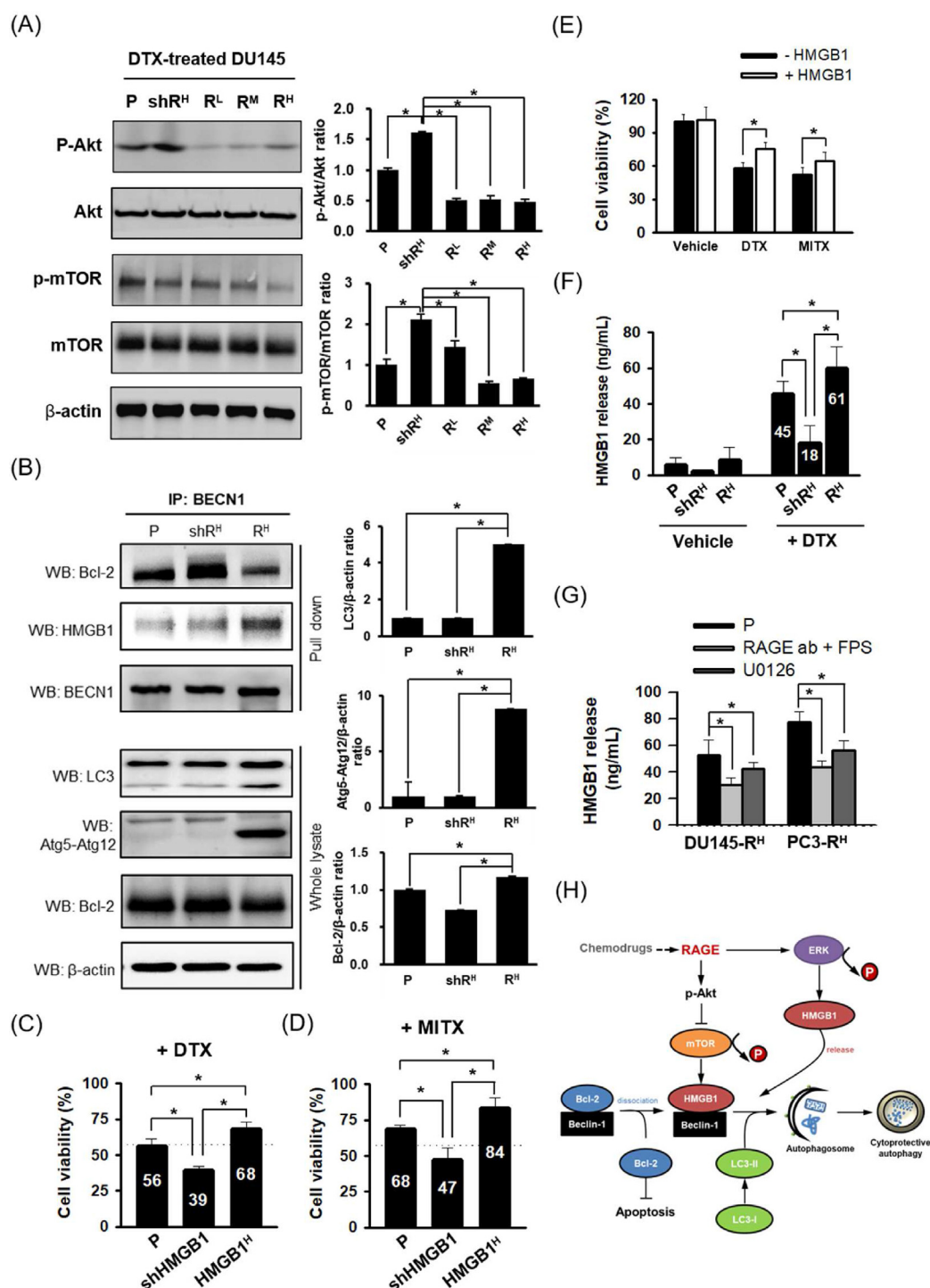
Fig. 4. HMGB1-induced autophagy involves the downregulation of AKT-mTOR signaling and the disruption of the Bcl-2−BECN1 complex via RAGE. (A) Western blot analysis of AKT and mTOR phosphorylation in the RAGE-overexpressed and knockdown clones of DU145 cells. The cells were treated with or without DTX (10 nM) for 24 h, and the cell lysates were analyzed with β-actin as a loading control. (B) The dissociation of Bcl-2 from BECN1 and the formation of the HMGB1−BECN1 complex were evaluated using co-IP assays. Protein extracts were immunoprecipitated with the BECN1 antibody at a dilution of 1:1000, followed by probing the immunocomplexes using western blotting to detect the presence of Bcl-2 and HMGB1 antibodies. The relative expression of proteins was quantified densitometrically and calculated according to the reference bands of the loading control. Targeted knockdown of HMGB1 increased sensitivity to chemodrugs in PCa cells, whereas overexpression of HMGB1 counteracted these effects. HMGB1-overexpressed (HMGB1^H) and knockdown (shHMGB1) clones of DU145 cells were treated with DTX (C) and MITX (D) for 24 h, and the cell viability was measured using an MTS assay. (E) HMGB1 treatment decreased the effectiveness of chemodrugs. The cells were pre-incubated with HMGB1 (10 μg/mL) for 6 h and then treated with DTX or MITX for another 24 h. Cell viability was measured by an MTS assay. (F)

*RAGE regulated HMGB1 release in response to the chemodrug challenge. The cells were treated with DTX for 24 h, and the release of HMGB1 in cell culture media was measured using an HMGB1 ELISA assay kit. (G) RAGE regulated HMGB1 release under chemodrug stress. DU145-R^H and PC3-R^H cells were pretreated with RAGE (a mixture of anti-RAGE neutralizing antibody and FPS-ZM1) or ERK (U0126, 10 μM) inhibitors for 6 h and then treated with DTX for another 24 h. Cell viability was measured. The inhibition of RAGE and ERK significantly attenuated DTX-mediated HMGB1 release. (H) Mechanistic investigation revealed that RAGE overexpression increased autophagy and limited apoptosis, resulting in PCa cell survival under chemodrug stress. RAGE-mediated autophagy was associated with decreased phosphorylation of Akt/mTOR and increased HMGB1−BECN1 complex formation. RAGE and downstream ERK were involved in the regulation of HMGB1 release. Data shown represents the means ± SD from three independent experiments. *P < 0.05 indicated statistically significant differences between groups. Co-IP, co-immunoprecipitation; IP, immunoprecipitation; WB, western blotting.*

HMGB1-overexpressing clone showed a 126% increase in HMGB1 release relative to the P cells, while the shHMGB1 clone HMGB1 release was reduced to 40% of that of the P cells. In the absence of DTX, the HMGB1 release returned to basal levels, and there were no statistically significant differences in HMGB1 release among these cells (P > 0.05). As the blockade of RAGE and ERK may contribute to the increased susceptibility to chemodrugs (Fig. 2F), we hypothesized that the chemoresistance actions of PCa cells were linked to the modulation of HMGB1 by RAGE and its downstream ERK. As shown in Fig. 4G, the inhibition of RAGE and ERK significantly attenuated DTX-mediated HMGB1 release (P < 0.05). These findings suggested that RAGE promotes protective autophagy by regulating Akt/mTOR phosphorylation, stimulating HMGB1 release, and dissociating the Bcl-2−BECN1 complex, which aids in HMGB1-BECN1 complex formation. HMGB1 appeared to be mediated by ERK in RAGE-overexpressed PCa cells (Fig. 4H).

3.5. Overexpression of RAGE induces epithelial−mesenchymal transition (EMT) and promotes invasiveness, cancer stem cell (CSC)−like properties, and tumorigenesis in xenograft mouse models

Morphological observation of RAGE-overexpressed and knockdown cells showed that the original cobblestone morphology of tight cell−cell contacts in parental cells was gradually changed to a long spindle shape as RAGE expression increased (Fig. 5A). This may allow cells to become polarized and lose cell−cell adhesion and junctions. Notably, when these spindle-like cells were subjected to RAGE knockdown, the cell morphology was restored to a near-parental type as observed in both the DU145 and PC3 cells (Fig. 5A). We postulated that these morphological changes might be associated with EMT. Fig. 5B showed that RAGE overexpression decreased the expression of E-cadherin while increasing the expression of N-cadherin and vimentin. The knockdown of RAGE counteracted these effects, which moved along to a parental phenotypic spectrum. The quantitative comparisons of the relative intensities of the E-cadherin, N-cadherin, and vimentin are shown in Fig. 5C−E, respectively.

We further evaluated the invasive potential of AGEs and RAGE on PCa cells using the invasion transwell assay. The results showed that cells with high RAGE expression degraded matrigel, and were more transwell invasive than P cells. In contrast, RAGE knockdown abolished the invasiveness significantly (Fig. 5F, P < 0.05). GA-derived AGEs, CML, and CEL could stimulate DU145 cells to become more invasive among the AGE compounds (Fig. 5G).

This study stained PCa cells with Hoechst 33342 and PI to identify their CSC characteristics by flow cytometry. Fig. 5H showed that the RAGE-overexpressed R^H clone had 8% higher SP than P cells (2.2%), whereas RAGE knockdown (shR^H) decreased its SP to 1.7%. The results revealed that overexpression of RAGE could stimulate the activity of ABC transporters and aid in xenobiotic efflux, which may lead to chemoresistance of PCa cells. Another CSC characteristic is high ALDH activity [20], and the ALDEFLOUR assay was used in this study for the fluorescent labeling of cells with high ALDH activity. The results showed in Fig. 5I, ALDH activity was increased in R^H cells and decreased in shR^H subclones. After subcutaneous grafting of the R^H clone in NON/SCID mice for 4 weeks, the tumor signal intensity was 4.8 and 2.4 times higher than the P and shRAGE^H subclones, respectively, as indicated in the mouse xenograft experiment (Fig. 5J). We further sorted SP and non-SP cells from the DU145-R^H clone and then subcutaneously injected the cells into the flanks of nude mice. After 10 weeks, the luminescence intensity of the SP group was 14.1 and 1.4 times higher than that of the non-SP and total population (R^H) groups, respectively (Fig. 5K). These *in vivo* results indicate that RAGE may drive CSC traits and contribute to the increased tumor-initiating capacity of advanced PCa.

3.6. The survival rate and malignancy of PCa are associated with CML and RAGE expressions

We collected 72 surgically resected PCa tissues and investigated the correlation of the CML and RAGE expression levels with clinicopathologic parameters in
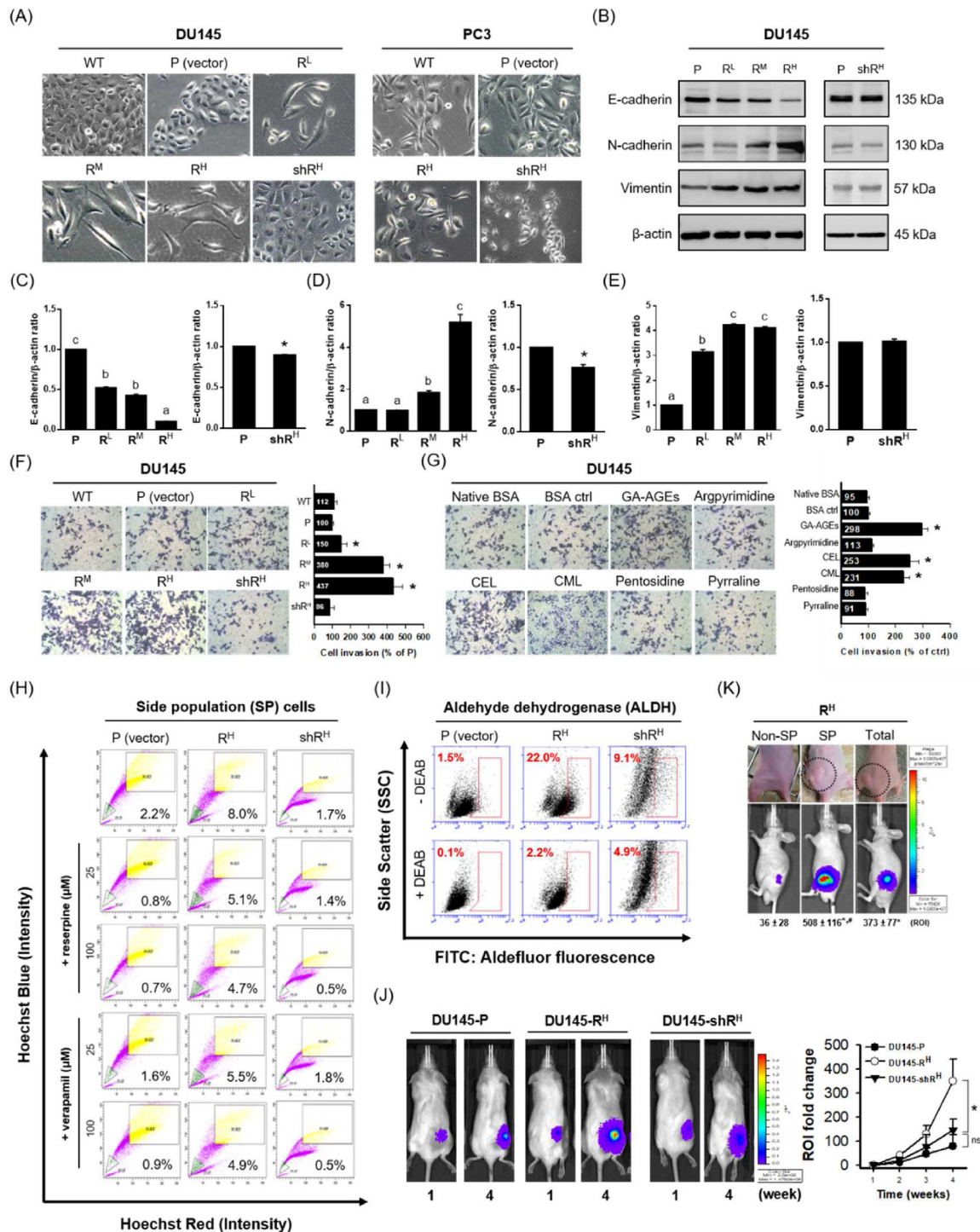
Fig. 5. *RAGE overexpression increases EMT, invasiveness, CSC-like properties, and tumorigenicity of PCa cells. (A) The cell morphology of RAGE-overexpressed and knockdown cells was observed under a phase-contrast microscope. Cell morphology was progressively changed from cuboidal epithelial morphology into an elongated and spindle-like mesenchymal shape with increasing expression of RAGE. (B) Western blot analysis of E-cadherin (epithelial marker), N-cadherin, and vimentin (mesenchymal markers) from cell lysates with β-actin as a loading control. The quantitative comparisons of relative intensities of the E-cadherin, N-cadherin, and vimentin are shown in Fig. 5C, D, and E, respectively. (F) RAGE overexpression and (G) AGE treatment promoted PCa cell invasion. DU145 cells were treated with GA-derived AGEs (500 μg/mL) or AGE compounds (250 nM), and the cell invasiveness was examined in Matrigel-coated transwell cell culture chambers. Invasive cells were visualized using crystal violet staining. (H) Analysis of SP cells in RAGE-overexpressed and knockdown DU145 cells. The populations of SP cells were detected using FACS analysis before and after treatment with verapamil and reserpine. SP cells were marked by black lines to show the proportion of SP cells among the total living cells. Flow cytometry demonstrated a very high percentage of Hoechst-Low SP cells in RAGE-overexpressed cells (R^H), whereas SP was*

dramatically decreased under RAGE was knockdown (shR^H). R^H cells had the highest percentage of SP fractions, whereas the shRAGE clone had lower SP fractions than that of P controls. (I) Determination of ALDH activity in RAGE-overexpressed and knockdown cells stained with ALDE-FLUOR reagent. Diethylaminobenzaldehyde (DEAB), an ALDH inhibitor, was used as a negative control. Flow cytometry data were illustrated as ALDH activity vs. side scatter signal (SSC). (J) RAGE modulated tumor growth in vivo. DU145 parental, R^H, and shR^H cells were subcutaneously injected into the flank of NOD/SCID mice (n = 5 per group). The tumor signals were detected using an IVIS Spectrum In Vivo Imaging System and quantified as the ROI fold change. (K) The SP and non-SP cells from the DU145-R^H clone were sorted using flow cytometry and then subcutaneously injected the cells into the flanks of nude mice at a density of 1 × 10^4 cells with matrigel. After 10 weeks, the luminescence intensity of the SP group was measured by the IVIS Spectrum In Vivo Imaging System as described above. Data shown represents the means ± SD from three independent experiments. ALDH, aldehyde dehydrogenase; DEAB, diethylaminobenzaldehyde; ROI, region of interest; SP, side population; WT, wild type.

patients with prostate adenocarcinoma. Patients with PCa were classified into low- and high-expression groups based on the IHC staining scores. IHC revealed markedly increased CML and RAGE expression levels in PCa tissues compared with those in adjacent normal tissues (Fig. 6A and B). The Kaplan–Meier analysis with the log-rank test revealed that high CML (P = 0.008, Fig. 6C) and RAGE (P = 0.011, Fig. 6D) expression levels were correlated with poor OS. Table 1 illustrated that the increased expression levels of CML and RAGE in PCa tissues were positively related to the Gleason score and prognostic group and negatively correlated with the 7-year OS. CML expression was also correlated with the disease stage, whereas RAGE expression was correlated with age. The 7-year OS rates for CML and RAGE were 40.9% and 36.4% in the high-expression groups, versus 59.1% and 63.6% in the low-expression groups, respectively (P < 0.05).

4. Discussion

The main aim of this study was to examine whether the AGE-RAGE axis is involved in PCa pathogenesis. Given that specific dietary patterns are associated with PCa risk [21,22], we hypothesized that both AGEs and RAGE are tumor-promoting agents that facilitate the progression of PCa. Several lines of evidence support this hypothesis. First, certain AGEs promote proliferation, invasion, and chemoresistance in human PCa cells. As AGEs might exert physiological consequences through the signaling cascade triggered by AGE-RAGE ligation, we further examined the function of RAGE on the hallmarks of PCa. By generating stable RAGE overexpression and knockdown cells from androgen-independent, highly invasive PCa cells, this study demonstrated that RAGE could facilitate the chemoresistance of PCa cells by triggering cytoprotective autophagy and evading apoptosis. Second, RAGE-overexpressed cells could undergo EMT, exhibit CSC-like properties, and be more tumorigenic than parental cells in xenograft mice models. In contrast, RAGE knockdown interfered with these cancer hallmarks. Notably, prostatic CML and RAGE expression levels exhibited close

association with malignancy and survival rates in patients with PCa. These findings revealed that the AGE-RAGE axis could be a prognostic factor for evaluating PCa.

This study provided a possible mechanism by which AGEs implicated in cancer progression is via the activation of RAGE. Except in the lungs, RAGE expression is relatively low in most tissues; however, RAGE can be activated at sites of inflammation [23]. The engagement of RAGE with AGEs could activate the NF-κB and TGF-β signaling, eliciting the release of proinflammatory cytokines and ROS generation, both of which are tumor-promoting factors for cancer [14,23]. Distinct AGEs, including CML, CEL, GA-, and GOA-derived AGEs, have been shown to bind to the extracellular V domain of RAGE and activate downstream MAPK signaling, triggering adhesion molecule expression and cytokine release. These AGEs are considered glycotoxins that could cause pathophysiological changes and aid in the development of cancers and chronic diseases [4,8,24]. In the A549 lung cancer cell line, GA-derived AGEs interact with RAGE and induce cell proliferation and migration [25]. Treating GLU-derived AGEs promotes cell migration and invasion of human gastric cancer cells through RAGE-mediated ERK phosphorylation [26]. In addition to AGEs, other prominent ligands can bind to and activate RAGE, such as amphoterin [27], HMGB1 [28], and S100 family protein [29]. Previous studies showed that GA-derived AGEs activate MAPK/NF-κB signaling and induce the nuclear translocation of STAT3 and β-catenin, enhancing invasive and migratory activities of HCT116 colon cancer cells. Additionally, GA-derived AGEs stimulate human mononuclear cells to secrete pro-carcinogenic factors and promote the proliferation of HCT116 colon cancer cells [30].

Under stress, PCa cells trigger autophagy to maintain cell survival [31]. In response to chemotherapy or H$_2$O$_2$ challenges, pancreatic cancer cells trigger autophagy via RAGE [32,33]. However, no studies have been conducted to determine if AGEs affect the phenomenon. Our study found that specific AGEs, including CML, CEL, and GA-derived AGEs, could enhance DTX resistance in both androgen-dependent and -independent PCa cells. sRAGE (a RAGE decoy)
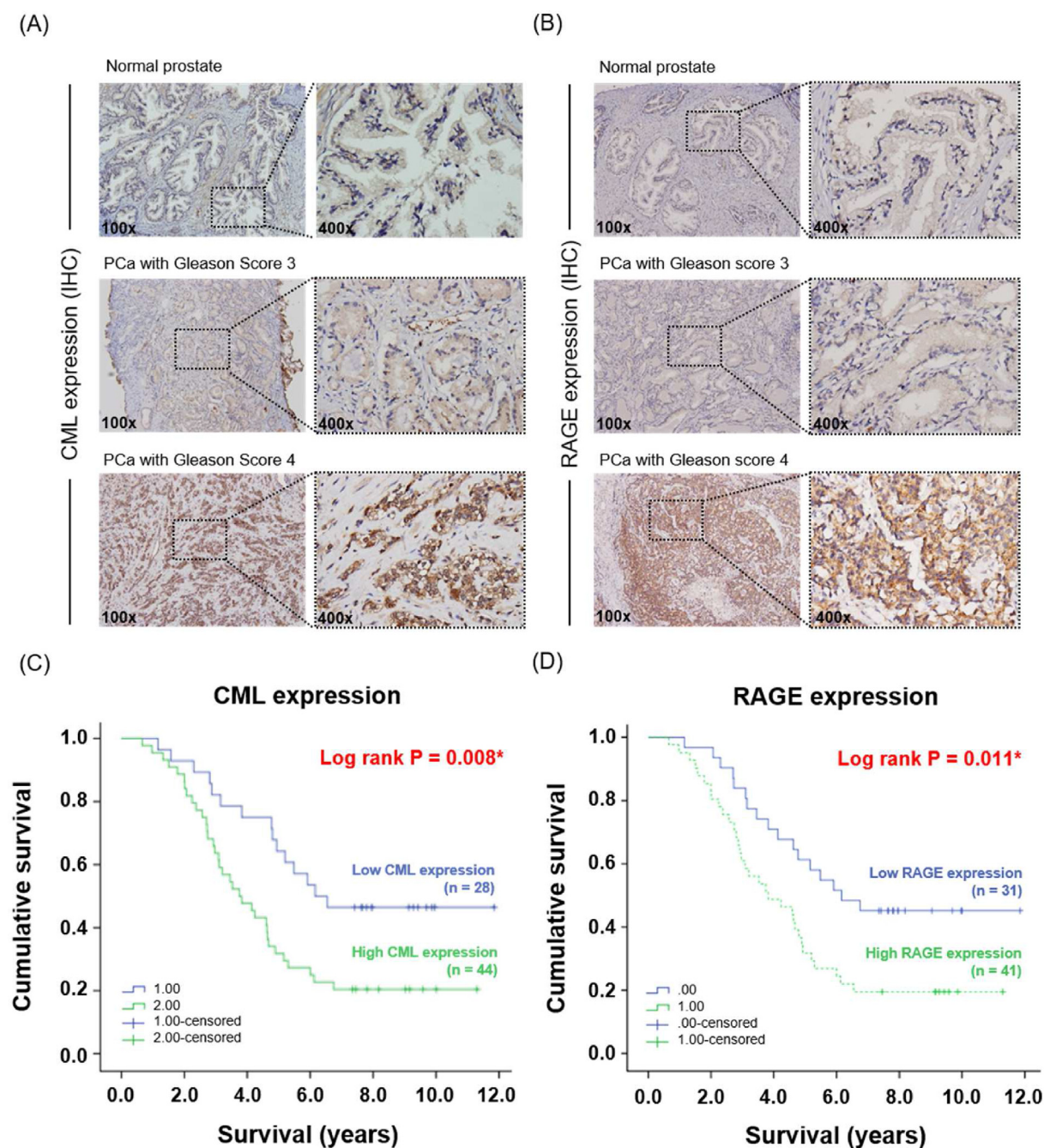
Fig. 6. Elevated CML and RAGE expression levels in prostate adenocarcinoma were associated with decreased survival rates in patients with PCa. (A) IHC analysis of CML and RAGE expression levels in normal and PCa tissues (Gleason score 3 and 4). (B) The Kaplan−Meier curves illustrating the OS rates of patients with PCa were related to the expression of CML (P = 0.008) and RAGE (P = 0.011). Analysis was performed using 72 PCa samples, and survival curves were compared with the log-rank test. IHC, immunohistochemical; OS, overall survival.

counteracted CML-mediated chemoresistance, implying a critical role of RAGE in resisting cell death. A previous study showed that the PI3K-Akt-mTOR and MAPK signaling pathways are upregulated in paclitaxel-resistant DU145 cells. Treatment with LY294002 or PD98059 renders these cells more sensitive to chemotherapeutic agents [34]. Based on these findings, PI3K-Akt-mTOR and ERK could be upstream signaling factors that modulate autophagy in PCa cells.

The present study provided evidence of molecular interactions among Bcl-2, BECN1, and HMGB1 by co-IP. We found that HMGB1 competes with Bcl-2, leading to HMGB1−BECN1 complex formation and maintaining cells in a self-defense status of anti-apoptosis and prone to autophagy under stress

Table 1. Clinicopathologic correlation of human prostate adenocarcinoma with CML and RAGE expression levels.

Parameter	CML expression (n = 72)				RAGE expression (n = 72)			
	Low-expression no. (%)	High-expression no. (%)	Total	P value[a]	Low Expression no. (%)	High Expression no. (%)	Total	P value
Age								
<75	14 (36.8)	24 (63.2)	38	0.706	11 (28.9)	27 (71.1)	38	**0.011***
≥75	14 (41.2)	20 (58.8)	34		20 (58.8)	14 (41.2)	34	
Gleason score								
<7	15 (68.2)	7 (31.8)	22	**0.003***	16 (72.7)	6 (27.3)	22	**0.003***
=7	8 (25.8)	23 (74.2)	31		8 (25.8)	23 (74.2)	31	
>7	5 (26.3)	14 (73.7)	19		7 (36.8)	12 (63.2)	19	
Prognostic group								
1	15(68.2)	7 (71.8)	22	**0.022***	16 (72.7)	6 (27.3)	22	**0.000***
2	4 (25.0)	12 (75.0)	16		1 (6.3)	15 (93.7)	16	
3	4 (26.7)	11 (73.3)	15		7 (46.7)	8 (43.3)	15	
4	1 (25.0)	3 (75.0)	4		3 (75.0)	1 (25.0)	4	
5	4 (26.7)	11 (73.3)	15		4 (26.7)	11 (73.3)	15	
T status								
T1	8 (61.5)	5 (38.5)	13	0.092	9 (69.2)	4 (30.8)	13	0.066
T2	8 (44.4)	10 (55.6)	18		7 (38.9)	11 (61.1)	18	
T3	8 (24.2)	25 (75.8)	33		10 (30.3)	23 (69.7)	33	
T4	4 (50.0)	4 (50.0)	8		5 (62.5)	3 (37.5)	8	
Lymph node metastasis								
No	24 (42.9)	32 (57.1)	56	0.196	26 (46.4)	30 (53.6)	56	0.280
Yes	4 (25.0)	12 (75.0)	16		5 (31.3)	11 (68.7)	16	
Distant metastasis								
No	20 (46.5)	23 (53.5)	43	0.106	21 (49.8)	22 (51.2)	43	0.228
Yes	8 (27.6)	21 (72.4)	29		10 (34.5)	19 (65.5)	29	
Stage								
I, II	14 (56.0)	11 (44.0)	25	**0.030***	13 (52.0)	12 (48.0)	25	0.264
III, IV	14 (29.8)	33 (70.2)	47		18 (38.3)	29 (61.7)	47	
Survival								
≤7 y	15 (30.0)	35 (70.0)	50	**0.020***	17 (34.0)	33 (66.0)	50	**0.019***
>7 y	13 (59.1)	9 (40.9)	22		14 (63.6)	8 (36.4)	22	

[a] The P value was analyzed by Pearson Chi-Square. Statistically significant P values are shown in bold. CML, Nε-(carboxymethyl)-lysine. no., number. RAGE, receptor for advanced glycation end product.

conditions. HMGB1 is a damage-associated molecular pattern molecule that can be actively released under stress or passively during cell death due to cell membrane rupture. Increased HMGB1 expression is observed in breast, colon, melanoma, pancreatic, and prostate cancer [35]. Kang et al. [36] pointed out that HMGB1 released by pancreatic cancer cells could bind to RAGE and promote ERK phosphorylation to facilitate mitochondrial ATP synthesis and maintain the continuous proliferation of cancer cells. Following this, we postulated that under chemodrug challenge, HMGB1 could be a key factor released from RAGE-overexpressed cells that acts in protective autophagy induction.

RAGE-mediated EMT, invasiveness, and cancer stemness may contribute to PCa aggressiveness, since EMT and stemness are linked to cancer chemoresistance, metastasis, and tumorigenic capacity [37]. Approximately 75−80% of castration-resistant PCa cells exhibit an EMT phenotype and the stem cell marker CD133 [38]. Our cellular experiments found that CML, CEL, and GA-derived AGEs enhanced the invasiveness of PCa cells. Notably, the cell morphology of RAGE-overexpressed cells changed to a long spindle shape, which is concurrent with the loss of cell−cell contacts and E-cadherin expression and underwent an upregulation of N-cadherin and vimentin. Previous studies showed that HMGB1 could trigger EMT and facilitate migration and invasion in DU145 cells via the Cdc42/GSK-3β/Snail pathway, whereas the knockdown of HMGB1 blocked EMT characteristics [39]. Here, the *in vivo* xenograft experiments further demonstrated that RAGE displayed tumor-promoting effects, whereas RAGE knockdown suppressed tumorigenesis and CSC stemness. These findings suggest that EMT properties may contribute to the invasiveness and stemness of RAGE-overexpressed PCa cells.

To our knowledge, AGEs have not been studied for their effects on PCa, and most studies have focused on the association between circulating levels of AGEs and PCa risk [40]. This study

collected prostate tissue specimens from 72 patients with PCa and a new prognostic grade group system for PCa proposed by the WHO [41] was adopted in conjunction with the Gleason score in this study. Our results revealed positive correlations between high CML and RAGE expression levels with more aggressive and poor clinical outcomes. These clinical data are consistent with the preclinical findings of the present study. A 10.5-year-long prospective study of 2193 pancreatic cancer patients found that dietary CML intake increased the risk of developing pancreatic cancer [42]. RAGE is preferentially highly expressed in poorly differentiated gastric adenocarcinomas and is closely associated with the invasiveness and lymph node metastasis of gastric cancer [43]. In a related PCa study, Ishiguro et al. [27] found that, in surgically resected human prostate tissues, RAGE mRNA expression in PCa was higher than that in normal prostate tissues. In a prospective case−control study that recruited 24 PCa cases and 24 healthy controls, Yang et al. [40] found that high levels of plasma CML were associated with an increased risk of PCa.

In conclusion, this study suggests that the AGE-RAGE axis plays a critical role in PCa progression and aggressiveness. Prostatic AGEs and RAGE expression levels are associated with PCa prognosis. Adherence to a reduced-AGE diet and targeting RAGE could be potential approaches to complement and synergize with the current PCa therapies.

Conflict of interest

The authors declare no conflict of interest.

Acknowledgments

Appendix. Supporting information

Supplementary materials and methods

Preparation and characterization of AGE-BSA

Preparation of GLU-, GA-, GO-, GO, and MG-derived AGE was based on the work of Takeuchi et al. [15]. BSA (25 mg/mL) was incubated at 37 °C for 14 days with 0.1 M of different glycated agents (GLU, GA, GOA, GO, and MG) in 0.2 M sodium phosphate buffer (pH 7.4), followed by using Disposable PD-10 Desalting Columns (Sigma−Aldrich) and dialysis to remove low molecular weight reactants and aldehydes. After that, Pierce High Capacity Endotoxin

Removal Spin Column (Thermo Fisher Scientific) was used to remove the endotoxins. AGE-BSA was lyophilized and stored at −20 °C. The endotoxin levels of each AGE-modified BSA sample were determined to be consistently below 1 EU/mL as detected using a ToxinSensor Chromogenic LAL Endotoxin Assay Kit (L00350, GenScript, Piscataway, NJ, USA). BSA incubated without a glycated agent was used as an unglycated control. The glycation levels of AGEs-BSA were estimated as the browning index (absorbance at 420 nm) and AGE-specific fluorescence intensity (Ex. 355 nm/Em 405 nm) using a FLUOstar galaxy fluorescence plate reader (BMG Lab Technologies, Offenburg, Germany), based on our previous studies [16, 30]. Protein crosslinking and aggregation were determined using sodium dodecyl sulfate polyacrylamide gel electrophoresis (SDS-PAGE) [16] (Fig. S1).

Cell viability

Cells were seeded in 96-well plates (5×10^3 cells/well) for the cell viability assessment, 100 mm Petri dishes ($5−10 \times 10^6$ cells) for the Western blot and immunofluorescence, and 4-well chamber slides (3×10^4 cells/slide) for transmission electron microscopy (TEM). Cell viability was measured using the CellTiter 96 AQueous One Solution Cell Proliferation Assay (Promega, Madison, WI, USA), as per the manufacturer's instructions. To evaluate chemodrug-induced toxicity, PCa cells were treated with docetaxel (DTX) and mitoxantrone (MTX). The IC_{50} for the DU145 and PC3 cells was 7.2 and 12.2 nM DTX, respectively, while the IC_{50} of MITX was 4.0 and 1.6 μM for these cell lines, respectively. The stock solutions of chemodrugs were prepared in DMSO, and DMSO at 0.1% served as a vehicle control. To examine whether AGEs promoted PCa cell proliferation, five AGE-BSA (GLU-derived AGEs, GA-derived AGEs, GOA-derived AGEs, GO-derived AGEs, and MG-derived AGEs) and five AGE compounds (argpyrimidine, CEL, CML, pentosidine, and pyrraline) were incubated with PCa cells for 48 h. The chemodrug resistance effects of AGE compounds (0−250 nM) on DTX and MITX in PCa cells were tested.

Plasmids and stable transfections

To generate stable RAGE and HMGB1 over-expression cells, 1 μg of the pUNO1-hager and pUNO1-hHMGB1 plasmids (#puno1-hager and #puno1-hhmgb1-s, InvivoGen, San Diego, CA, USA) were transfected into PC3 and DU145 cells using the Lipofectamine 3000 Transfection Reagent (Thermo Fisher Scientific) as described previously [44]. The cells were cultured with blasticidin (5 μg/mL, ant-bl-1, InvivoGen) for 4 weeks to obtain a single-cell clone.

The pUNO1-mcs plasmid (#puno1-mcs, InvivoGen) was an empty control vector. To generate RAGE- and BECN1-genetic silencing cells, DU145 and PC3 cells were transfected with BECN1 shRNA plasmids (sc-29797-SH, Santa Cruz Biotechnology) for 48 h. Cells stably expressing targeted shRNA were isolated using puromycin selection (5 μg/mL, ant-pr-1, InvivoGen). Non-targeting control shRNA (sc-108060) served as a control. HMGB1 stable knockdown DU145 cells as described previously [39]. The plasmids and transfection reagent were diluted in Gibco Opti-MEM Reduced Serum Media (Thermo Fisher Scientific). Total protein lysates (20 μg) from antibiotic-selecting cells were analyzed using western blotting or immunofluorescence for monitoring target protein expression. In this study, RAGE-transfected DU145 cells were classified as RAGE low-expressing (R^L) clones, medium-expressing (R^M) clones, and high-expressing (R^H) clones based on the RAGE expression level. DU145-R^H clones were subjected to RAGE shRNA plasmid transfection to generate shR^H subclones for subsequent experiments (Fig. S2).

Immunoblotting and immunoprecipitation

For immunoblotting [16], cells were lysed using RIPA buffer (Bioman Scientific, Taiwan) with protease and phosphatase inhibitors (78447, Thermo Fisher Scientific). Total protein lysates (20 μg) were separated using SDS-PAGE, transferred to PVDF membranes, blocked in 5% non-fat milk in Tris-buffered saline with 0.1% Tween-20 (TBST), and subsequently probed with the indicated antibodies. Immune complexes were detected with horseradish peroxidase (HRP)-conjugated secondary antibodies, chemiluminescent HRP substrate (Millipore), and a Fusion Solo System (Vilber Lourmat, Germany). The protein concentration was measured using the Bio-Rad Protein Assay (#500-0006, Bio-Rad Laboratories, Hercules, CA, USA). For immunoprecipitation (IP), the cells were lysed using Pierce IP Lysis Buffer (87787, Thermo Fisher Scientific) with protease and phosphatase inhibitors (Thermo Fisher Scientific). Lysed proteins (50 μg) were IP with Dynabeads Protein G (10003D, Invitrogen, Carlsbad, CA, USA) for 2 h at 4 °C after coating with the indicated antibody according to the manufacturer's instructions. Briefly, 10 μg of anti-BECN1 antibody was added to the magnetic dynabeads (1.5 mg) for 30 min at 24 °C. The magnetic bead-protein complex was eluted and denatured by heating for 10 min at 70 °C, resuspended in SDS sample buffer, and the supernatant was loaded in gels to conduct SDS-PAGE and western blotting. Protein expression was measured densitometrically compared to the loading control reference band using ImageJ software.

Hematoxylin & eosin (HE) and immunohistochemistry (IHC) staining

Human prostate tissues were collected and stained with HE. Sections (4 μm) of formalin-fixed paraffin-embedded tissues were deparaffinized in xylene and rehydrated using graded ethanol. Antigen retrieval was performed by heating with citric acid buffer (10 mM, pH 6.0) at 100 °C for 20 min before incubating in a 3% H_2O_2 solution to block endogenous peroxidase activity. IHC staining of prostate tissue was performed using the EnVision + Dual Link System (Dako, Carpinteria, CA, USA) in accordance with the manufacturer's instructions. Tissue sections were blocked with 5% BSA for 30 min at RT and incubated with the anti-CML (1:100) and anti-RAGE (1:100) antibodies for 2 h at RT. Following incubation with a secondary biotinylated antibody, tissue sections were labeled using diaminobenzidine and counterstained with Mayer's hematoxylin. To determine the specificity of the primary antibodies, serial dilution testing was performed. In a double-blind setup, the IHC staining sections were scored using a semiquantitative scoring system by two independent histopathologists (Dr. Pei-Ru Wu and Dr. Kun-Tu Yeh). The CML and RAGE expressions were divided into low- and high-expression groups based on scores of 0−1 and 2−3, respectively. No cytoplasmic staining was scored as 0, mild cytoplasmic staining scored as 1, moderate cytoplasmic staining scored as 2, and strong cytoplasmic staining scored as 3.

Table S1. Listed of chemicals used in this study

Chemicals	Catalog number	Company
BSA (fatty acid-free)	A7030	Sigma−Aldrich
D-(+)-Glucose (GLU)	G7021	Sigma−Aldrich
Glyoxal (GO)	50649	Sigma−Aldrich
Methylglyoxal (MG)	M0252	Sigma−Aldrich
FPS-ZM1	553030	Sigma−Aldrich
Wortmannin	W1628	Sigma−Aldrich
Docetaxel (DTX)	01885	Sigma−Aldrich
Mitoxantrone (MTX)	M6545	Sigma−Aldrich
D-(+)-glyceraldehyde (GA)	453-17-8	BOC Sciences
Glycolaldehyde (GOA)	141-46-8	BOC Sciences
Argpyrimidine trifluoroacetic acid salt	SC1534	PolyPeptide
CEL	SC1506	PolyPeptide
CML	SC1505	PolyPeptide
Pentosidine trifluoroacetic acid salt	SC1535	PolyPeptide
Pyrraline	SC1559	PolyPeptide
sRAGE recombinant protein	RD272590100	Biovendor R&D
Hoechst 33342	62249	Thermo Fisher Scientific
Propidium iodide (PI)	P3566	Thermo Fisher Scientific
DAPI	ab228549	Abcam
HMGB1 recombinant protein	ab167718	Abcam

Table S2. Listed of antibodies used for western blotting and immunofluorescence analysis

| Antibody (target)	Catalog number	Company
Akt	MAB2055	Novus Biologicals
p-Akt	NB100-56749	Novus Biologicals
Beclin-1 (BECN1)	NB500-249	Novus Biologicals
ERK1/2	AF1576	Novus Biologicals
p-ERK1/2	AF1018	Novus Biologicals
HMGB1	NB100-2322	Novus Biologicals
p62	H00008878-M01	Novus Biologicals
E-cadherin	sc-8426	Santa Cruz Biotechnology
N-cadherin	sc-8424	Santa Cruz Biotechnology
ATG12-ATG5	#2630	Cell Signaling Technology
Bcl-2	#15071	Cell Signaling Technology
cleaved caspase-3	#9661	Cell Signaling Technology
GAPDH	#5174	Cell Signaling Technology
LC3B	#2775	Cell Signaling Technology
PARP	#9532	Cell Signaling Technology
mTOR	#2983	Cell Signaling Technology
p-mTOR	#2971	Cell Signaling Technology
vimentin	#5741	Cell Signaling Technology
β-actin	#4970	Cell Signaling Technology
CML	KAL-KH024	Cosmo Bio
RAGE	MAB5328	Millipore
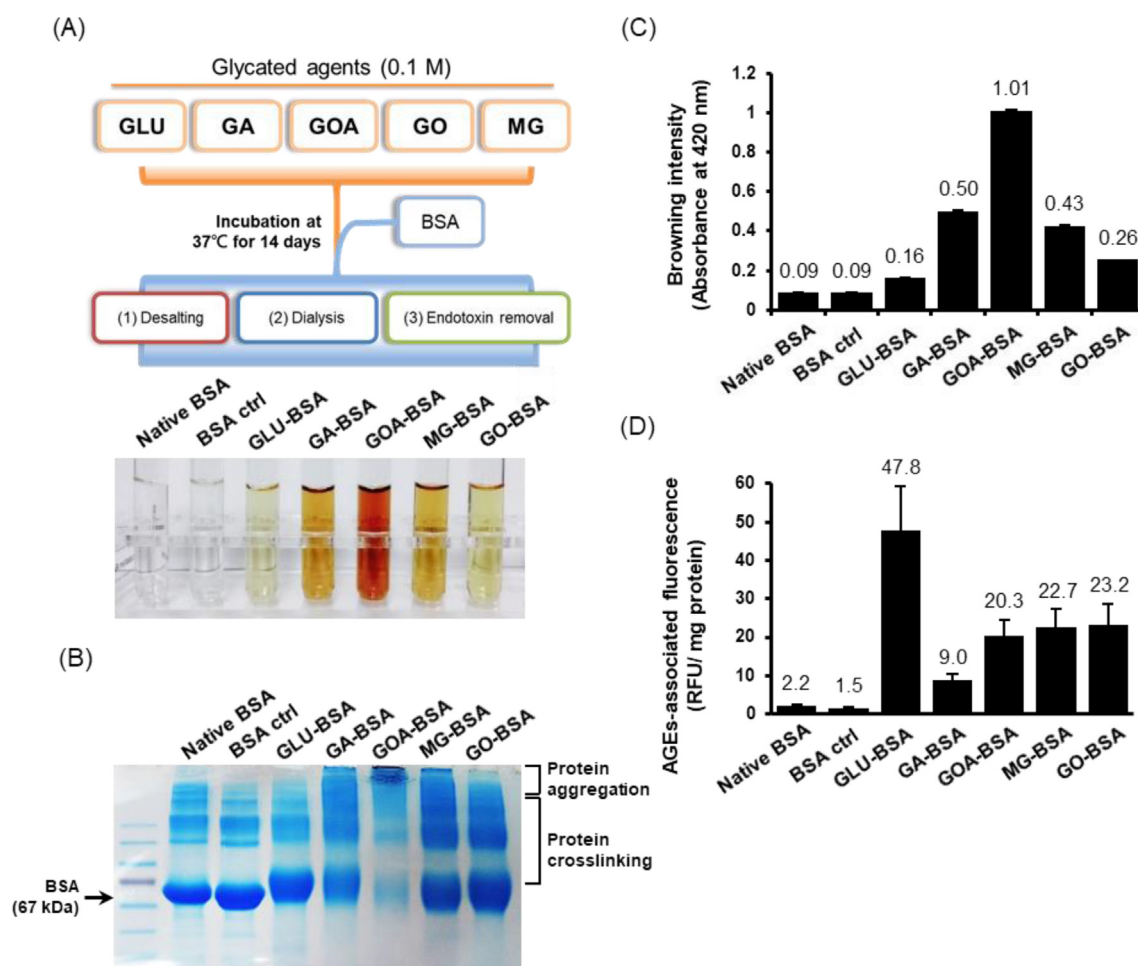
Fig. S1. Characteristics of the AGE-BSA proteins. (A) GLU-, GA-, GOA-, GO-, and MG-glycated BSA were prepared as described in the Supplementary Materials and Methods section. BSA incubated without a glycated agent was used as a control (BSA ctrl). (B) The crosslinking and aggregation of AGE-modified BSA were analyzed using SDS-PAGE and stained with Coomassie blue. The band corresponding to BSA (67 kDa) faded gradually, and the appearance of smeared and aggregated bands in the higher molecular weight range was attributed to the protein glycation. (C) The browning intensity used as an initial indicator of glycation was measured spectrophotometrically at 420 nm. (D) The AGE-associated fluorescence was measured in both BSA and AGEs-modified BSA by an excitation wavelength of 340 nm and an emission wavelength of 410 nm. Data shown represents the means ± SD from three independent experiments. GA, glyceraldehyde; GLU, glucose. GOA, glycolaldehyde; GO, glyoxal; MG, methylglyoxal; RFU, relative fluorescence unit.
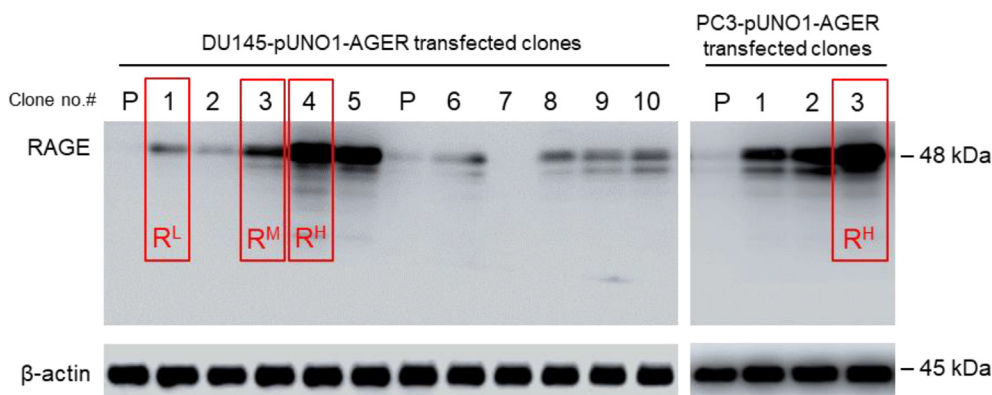
Fig. S2. Stable clone selection of the DU145 and PC3 cells after pUNO1-ager vector transfection. Western blots of ten clone lysates from DU145 and three clone lysates from PC3 cells using RAGE-specific antibody. For DU145 cells, clone #4 was chosen as high-RAGE expression (R^H), clone #3 as middle-RAGE expression (R^M), and clone #1 as low-RAGE expression (R^L). For PC3 cells, clone #3 was chosen as having high-RAGE expression clone (R^H). pUNO1-ager is an expression vector containing a human RAGE open reading frame. P, parental cells with empty vector (pUNO1-mcs) transfection.
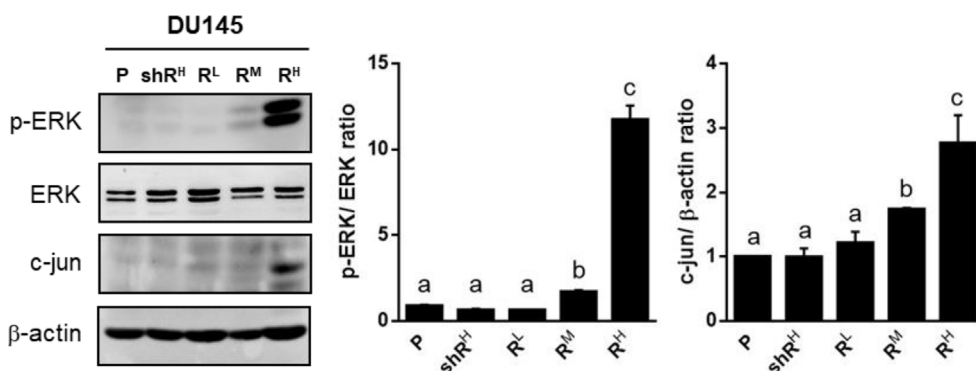

Fig. S3. Western blot analysis of ERK phosphorylation and c-jun protein expression in the RAGE-overexpressed and knockdown clones of DU145 cells. Stably RAGE-expressing DU145 cells were divided into low (R^L), middle (R^M), and high (R^H) clones based on the level of RAGE protein. R^H cells further subjected to shRAGE transfection were referred to as shR^H subclones. β-actin was used as the loading control. The results showed that ERK phosphorylation and c-jun protein expression were accompanied by RAGE overexpression. Data shown are the means ± SD from three independent experiments. Different letters indicate significant differences between groups ($P < 0.05$).

References

[1] Murata M. Browning and pigmentation in food through the Maillard reaction. Glycoconj J 2021;38:283−92.

[2] Nie C, Li Y, Qian H, Ying H, Wang L. Advanced glycation end products in food and their effects on intestinal tract. Crit Rev Food Sci Nutr 2022;62:3103−15.

[3] Uribarri J, Cai W, Sandu O, Peppa M, Goldberg T, Vlassara H. Diet-derived advanced glycation end products are major contributors to the body's AGE pool and induce inflammation in healthy subjects. Ann N Y Acad Sci 2005;1043:461−6.

[4] Takeuchi M, Sakasai-Sakai A, Takata T, Takino JI, Koriyama Y. Effects of toxic AGEs (TAGE) on human health. Cells 2022;11(14).

[5] Brownlee M, Michael. Advanced protein glycosylation in diabetes and aging. Annu Rev Med 1995;46:223−34.

[6] Thornalley PJ. Dicarbonyl intermediates in the maillard reaction. Ann N Y Acad Sci 2005;1043:111−7.

[7] Rabbani N, Xue M, Thornalley PJ. Dicarbonyl stress, protein glycation and the unfolded protein response. Glycoconj J 2021;38:331−40.

[8] Ahmad S, Khan H, Siddiqui Z, Khan MY, Rehman S, Shahab U, et al. AGEs, RAGEs and s-RAGE; friend or foe for cancer. Semin Cancer Biol 2018;49:44−55.

[9] Zawada A, Machowiak A, Rychter AM, Ratajczak AE, Szymczak-Tomczak A, Dobrowolska A, et al. Accumulation of advanced glycation end-products in the body and dietary habits. Nutrients 2022;14:3982.

[10] Stott-Miller M, Neuhouser ML, Stanford JL. Consumption of deep-fried foods and risk of prostate cancer. Prostate 2013;73:960−9.

[11] Nouri-Majd S, Salari-Moghaddam A, Aminianfar A, Larijani B, Esmaillzadeh A. Association between red and processed meat consumption and risk of prostate cancer: a systematic Review and meta-analysis. Front Nutr 2022;9:801722.

[12] Arroyo-Quiroz C, Brunauer R, Alavez S. Sugar-sweetened beverages and cancer risk: a narrative Review. Nutr Cancer 2022;74:3077−95.

[13] Shivappa N, Bosetti C, Zucchetto A, Montella M, Serraino D, La Vecchia C, et al. Association between dietary inflammatory index and prostate cancer among Italian men. Br J Nutr 2015;113:278−83.

[14] Eva TA, Barua N, Chowdhury MM, Yeasmin S, Rakib A, Islam MR, et al. Perspectives on signaling for biological- and processed food-related advanced glycation end-products and its role in cancer progression. Crit Rev Food Sci Nutr 2022;62:2655−72.

[15] Takeuchi M, Makita Z, Bucala R, Suzuki T, Koike T, Kameda Y. Immunological evidence that non-carboxymethyllysine advanced glycation end-products are produced from short chain sugars and dicarbonyl compounds in vivo. Mol Med 2000;6:114−25.

[16] Wu CH, Huang SM, Yen GC. Silymarin: a novel antioxidant with antiglycation and antiinflammatory properties in vitro and in vivo. Antioxidants Redox Signal 2011;14:353−66.

[17] Lin JA, Wu CH, Lu CC, Hsia SM, Yen GC. Glycative stress from advanced glycation end products (AGEs) and dicarbonyls: an emerging biological factor in cancer onset and progression. Mol Nutr Food Res 2016;60:1850−64.

[18] Tirino V, Desiderio V, Paino F, Papaccio G, De Rosa M. Methods for cancer stem cell detection and isolation. Somatic Stem Cells Meth Prot 2012:513−29.

[19] Edge SB, Compton CC. The American Joint Committee on Cancer: the 7th edition of the AJCC cancer staging manual and the future of TNM. Ann Surg Oncol 2010;17:1471−4.

[20] Greve B, Kelsch R, Spaniol K, Eich HT, Götte M. Flow cytometry in cancer stem cell analysis and separation. Cytometry 2012;81:284−93.

[21] Matsushita M, Fujita K, Nonomura N. Influence of diet and nutrition on prostate cancer. Int J Mol Sci 2020;21(4).

[22] Trudeau K, Rousseau M-C, Barul C, Csizmadi I, Parent M-É. Dietary patterns are associated with risk of prostate cancer in a population-based case-control study in montreal, Canada. Nutrients 2020;12:1907.

[23] Faruqui T, Khan MS, Akhter Y, Khan S, Rafi Z, Saeed M, et al. RAGE inhibitors for targeted therapy of cancer: a comprehensive Review. Int J Mol Sci 2022;24(1).

[24] Xue J, Rai V, Singer D, Chabierski S, Xie J, Reverdatto S, et al. Advanced glycation end product recognition by the receptor for AGEs. Structure 2011;19:722−32.

[25] Takino J-I, Yamagishi S-I, Takeuchi M. Cancer malignancy is enhanced by glyceraldehyde-derived advanced glycation end-products. J Oncol 2010;2010.

[26] Deng R, Mo F, Chang B, Zhang Q, Ran H, Yang S, et al. Glucose-derived AGEs enhance human gastric cancer metastasis through RAGE/ERK/Sp1/MMP2 cascade. Oncotarget 2017;8:104216.

[27] Ishiguro H, Nakaigawa N, Miyoshi Y, Fujinami K, Kubota Y, Uemura H. Receptor for advanced glycation end products (RAGE) and its ligand, amphoterin are overexpressed and associated with prostate cancer development. Prostate 2005;64:92−100.

[28] Gnanasekar M, Thirugnanam S, Ramaswamy K. Short hairpin RNA (shRNA) constructs targeting high mobility group box-1 (HMGB1) expression leads to inhibition of prostate cancer cell survival and apoptosis. Int J Oncol 2009;34:425−31.

[29] Siddique HR, Adhami VM, Parray A, Johnson JJ, Siddiqui IA, Shekhani MT, et al. The S100A4 oncoprotein promotes prostate tumorigenesis in a transgenic mouse model: regulating NFκB through the RAGE receptor. Genes Cancer 2013;4:224−34.

[30] Lin JA, Wu CH, Yen GC. Breadfruit flavonoid derivatives attenuate advanced glycation end products (AGEs)-enhanced colon malignancy in HCT116 cancer cells. J Funct Foods 2017;31:248−54.

[31] Ashrafizadeh M, Paskeh MDA, Mirzaei S, Gholami MH, Zarrabi A, Hashemi F, et al. Targeting autophagy in prostate cancer: preclinical and clinical evidence for therapeutic response. J Exp Clin Cancer Res 2022;41:105.

[32] Kang R, Tang D, Schapiro NE, Livesey KM, Farkas A, Loughran P, et al. The receptor for advanced glycation end products (RAGE) sustains autophagy and limits apoptosis, promoting pancreatic tumor cell survival. Cell Death Differ 2010;17:666−76.

[33] Kang R, Tang D, Livesey KM, Schapiro NE, Lotze MT, Zeh 3rd HJ. The Receptor for Advanced Glycation End-products (RAGE) protects pancreatic tumor cells against oxidative injury. Antioxidants Redox Signal 2011;15:2175−84.

[34] Liu Z, Zhu G, Getzenberg RH, Veltri RW. The upregulation of PI3K/Akt and MAP kinase pathways is associated with resistance of microtubule-targeting drugs in prostate cancer. J Cell Biochem 2015;116:1341−9.

[35] Sims GP, Rowe DC, Rietdijk ST, Herbst R, Coyle AJ. HMGB1 and RAGE in inflammation and cancer. Annu Rev Immunol 2010;28:367−88.

[36] Kang R, Tang D, Schapiro N, Loux T, Livesey K, Billiar T, et al. The HMGB1/RAGE inflammatory pathway promotes pancreatic tumor growth by regulating mitochondrial bioenergetics. Oncogene 2014;33:567−77.

[37] Mitra A, Mishra L, Li S. EMT, CTCs and CSCs in tumor relapse and drug-resistance. Oncotarget 2015;6:10697.

[38] Armstrong AJ, Marengo MS, Oltean S, Kemeny G, Bitting RL, Turnbull JD, et al. Circulating tumor cells from patients with advanced prostate and breast cancer display both epithelial and mesenchymal markersepithelial/mesenchymal markers on circulating tumor cells. Mol Cancer Res 2011;9:997−1007.

[39] Chang HY, Chen SY, Wu CH, Lu CC, Yen GC. Glycyrrhizin attenuates the process of epithelial-to-mesenchymal transition by modulating HMGB1 initiated novel dignaling pathway in prostate cancer cells. J Agric Food Chem 2019;67:3323−32.

[40] Yang S, Pinney SM, Mallick P, Ho SM, Bracken B, Wu T. Impact of oxidative stress biomarkers and carboxymethyllysine (an advanced glycation end product) on prostate cancer: a prospective study. Clin Genitourin Cancer 2015;13:e347−51.

[41] Humphrey PA, Ulbright TM, Reuter VE, Moch H. WHO classification of tumours of the urinary system and male genital organs. International Agency for Research on Cancer; 2016.

[42] Jiao L, Stolzenberg-Solomon R, Zimmerman TP, Duan Z, Chen L, Kahle L, et al. Dietary consumption of advanced glycation end products and pancreatic cancer in the prospective NIH-AARP Diet and Health Study. Am J Clin Nutr 2015;101:126−34.

[43] Kuniyasu H, Oue N, Wakikawa A, Shigeishi H, Matsutani N, Kuraoka K, et al. Expression of receptors for advanced glycation end-products (RAGE) is closely associated with the invasive and metastatic activity of gastric cancer. J Pathol 2002;196:163−70.

[44] Chen MC, Chen KC, Chang GC, Lin H, Wu CC, Kao WH, et al. RAGE acts as an oncogenic role and promotes the metastasis of human lung cancer. Cell Death Dis 2020;11:265.